IDENTIFICATION OF PLANETARY AND PROTO-PLANETARY NEBULAE CANDIDATES THROUGH *AKARI* INFRARED PHOTOMETRY

R. A. Márquez-Lugo[1,2], S. N. Kemp[1,2], G. Ramos-Larios[1,2], A. Nigoche-Netro[1,2], S. G. Navarro[1,2], and L. J. Corral[1,2]

ABSTRACT

We utilized photometric data from the space telescope *AKARI* to identify potential planetary nebulae (PNe) and proto-planetary nebulae (PPNe) candidates. Using the color-color diagram, we found a region with a high concentration of established PNe and PPNe, comprising about 95% of the objects. Based on this, we identified 67 objects within this region that lack definitive classification in existing literature, suggesting they are promising candidates. We conducted Spectral Energy Distribution (SED) analysis and morphological investigations using imagery from various observatories and satellites. Finally, we present a list of 65 potential PNe and PPNe candidates.

RESUMEN

Utilizamos datos fotométricos del telescopio espacial *AKARI* para identificar posibles candidatos a nebulosas planetarias (PNe) y proto-nebulosas planetarias (PPNe). Utilizando el diagrama de color-color, encontramos una región con una alta concentración de PNe y PPNe establecidas, que comprende aproximadamente el 95% de los objetos. Basados en esto, identificamos 67 objetos dentro de esta región que carecen de clasificación definitiva en la literatura existente, sugiriendo que son candidatos prometedores. Realizamos análisis de Distribución de Energía Espectral (SED) e investigaciones morfológicas utilizando imágenes de varios observatorios y satélites. Finalmente, presentamos una lista de 65 posibles candidatos a PNe y PPNe.

Key Words: infrared: ISM — planetary nebulae: general — stars: AGB and post-AGB

1. INTRODUCTION

The identification of extended planetary nebulae (PNe) has been carried out by morphological or spectral analysis (Pottasch 1984). However, in the case of unresolved sources, photometric methods, such as *IRAS* (Infrared Astronomical Satellite) color-color diagrams, have been employed (Pottasch et al. 1988; Preite-Martínez 1988; van de Steene & Pottasch 1993, 1995; Manchado et al. 1989; García-Lario et al. 1990; Ramos-Larios et al. 2009; Akras, Guzman-Ramirez, & Gonçalves 2019) or 2MASS (Two Micron All-Sky Survey) and *WISE* (Wide-Field Infrared Survey Explorer) for the identification and classification of symbiotic stars (Akras et

al. 2019). The available data from the infrared astronomical mission *AKARI* (Murakami et al. 2007) have been shown to be useful in the study of known PNe and proto-planetary nebulae (PPNe) (Cox, et al. 2009 a,b, 2011; Phillips & Márquez-Lugo 2011; Pollo, Takeuchi & Rybka 2011; Ohsawa, et al. 2012, 2016; Ueta, et al. 2019), which is why we have used photometric data from the *AKARI* Point Source Catalog (*AKARI* PSC) to identify new PNe and PPNe candidates.

We utilized widely recognized catalogues encompassing planetary nebulae (PNe), galaxies, young stellar objects (YSOs), main sequence and pre-main sequence stars, symbiotic stars, OH/IR stars, Herbig-Haro objects (HH), and HII compact regions. The objective was to pinpoint the positions of these sources within an *AKARI* Point Source Catalogue (PSC) color-color diagram. Our focus was on iden-

---

[1]Instituto de Astronomía y Meteorología, Universidad de Guadalajara, Jalisco, México.

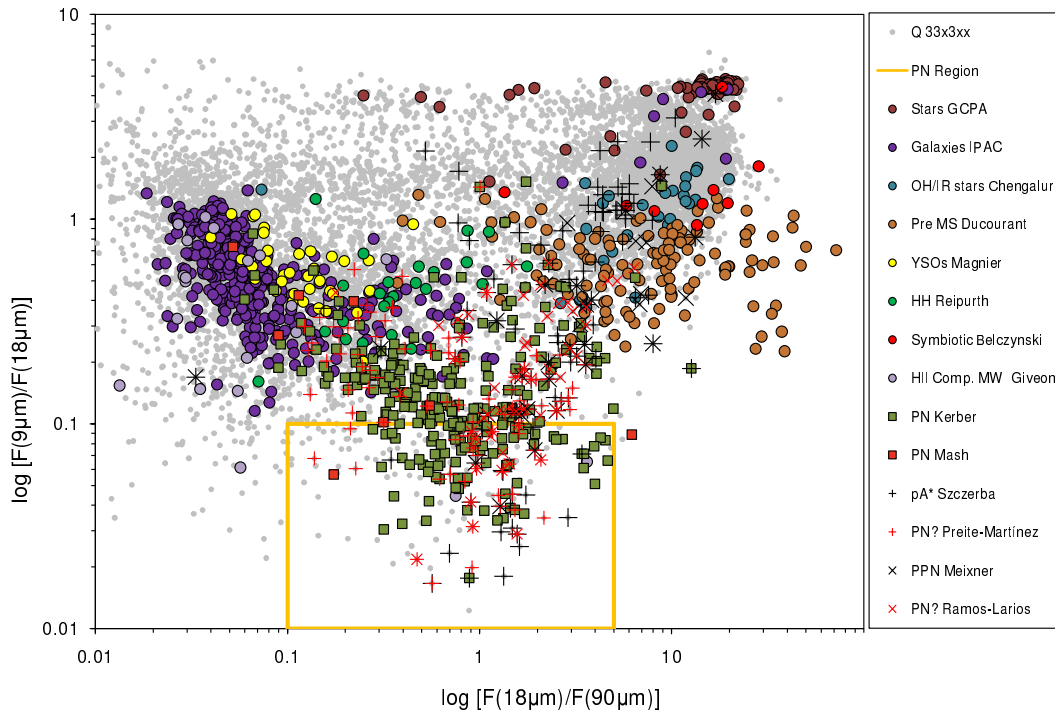[2]Departamento de Física, Universidad de Guadalajara, Jalisco, México.

Fig. 1. *AKARI* PSC color-color diagram. The *AKARI* PSC sources with Q33x3xx are shown as grey points, and the right hand panel indicates other, superimposed symbols (see text for details). The area delineated in yellow contains a concentration of PNe, PPNe, post-AGB stars, and candidates for all these categories, and excludes an enormous proportion of other types of astronomical objects. The color figure can be viewed online.

tifying a distinct region where planetary nebulae (PNe) are prominently featured and relatively segregated from other categories of astronomical entities.

2. OBSERVATIONS

The *AKARI* PSC photometry has been accessible to the public since March 2010. In addition, mission image data have been released, starting with the *AKARI* far-infrared all-sky survey maps, available since December 2014, and subsequently the *AKARI*/IRC Pointed Observation Images from March 2015 (IRC, InfraRed Camera). However, owing to the suboptimal resolution of *AKARI* images for the present study, we employed image data from other infrared and optical projects such as the *Spitzer Space Telescope*, The INT Photometric Hα Survey of the Northern Galactic Plane (IPHAS), 2MASS, and *WISE*. These alternative datasets were utilized to examine the spatial emission profiles of PNe candidates and, as a preliminary step, to analyze their morphology (for detailed information, refer to § 6).

To generate the color-color diagram for distinguishing between various types of astronomical objects, we employed photometry data from the PSC

of the *AKARI* space telescope (previously known as ASTRO-F or IRIS Infra Red Imaging Surveyor, launched on February 21, 2006). This dataset comprises two components: one obtained from the IRC featuring two bands centered at $9\mu m$ and $18\mu m$ (Ishihara et al. 2010), and the other from the Far-Infrared Surveyor (FIS) with four bands centered at $65\mu m$, $90\mu m$, $140\mu m$, and $160\mu m$ (Kawada et al. 2007).

For constructing the spectral energy distributions (SEDs) we utilized data not only from *AKARI*, but also from: US Naval Observatory B catalogue (USNO-B), compiled from the digitalisation of various photographic sky surveys plates by the Precision Measuring Machine (PMM), located at the US Naval Observatory Flagstaff Station (NOFS), from 350 nm to 900 nm between 1949 and 2002 (Monet et al. 2003); 2MASS, with three bands J ($1.25\mu m$), H ($1.65\mu m$) and K ($2.17\mu m$) from the 1.3 m telescopes at Mount Hopkins and Cerro Tololo Inter-American Observatory (CTIO) Chile (Kleinmann 1992); the Deep Near Infrared Southern Sky Survey (DENIS) (Fouqué et al. 2000) with three bands i ($0.802\mu m$), J ($1.248\mu m$) and K_s ($2.152\mu m$); the Midcourse Space Experiment (MSX) (Egan & Price

1996), from the telescope SPIRIT III aboard the Ballistic Missile Defense Organization (BMDO) with the bands A (8.28μm), C (12.13μm), D (14.65μm) and E (21.3μm) and the Infrared Array Camera (IRAC) (Fazio et al. 2004) aboard the *Spitzer Space Telescope* with the bands I1 (3.6μm), I2 (4.5μm), I3 (5.8μm) and I4 (8.0μm).

The resolution of the images of the *AKARI* far-infrared all-sky survey maps, with pixel sizes of the detectors of 26.8″×26.8″ for the short wavelength bands N60 and WIDE-S, and 44.2″×44.2″ for the long wavelength bands N160 and WIDE-L (Doi, et al. 2015) is too poor to study the morphology and vicinity of the candidates; therefore *WISE* (Wide-Field Infrared Survey Explorer, Wright et al. 2010) images were used for this purpose. Furthermore, radial emission profiles of sources were derived from *Spitzer* IRAC, 2MASS and IPHAS data.

3. SEARCHING FOR CANDIDATES

3.1. *The* AKARI *Point Source Catalogue*

The *AKARI* PSC comprises two components: the *AKARI* FIS Bright Source Catalogue (Yamamura et al. 2010) and the *AKARI* IRC Point Source Catalogue (Ishihara et al. 2010). The AKARI IRC Catalogue encompasses data from two bands centered at 9μm and 18μm. The 9μm band includes information for 844,649 sources, while the 18μm band comprises data for 194,551 sources In total, there is information for 870,973 unique sources, with 168,227 sources appearing in both bands. On the other hand, the *AKARI* FIS Catalogue provides photometric data for 427,071 sources, each observed in at least one of the four bands centered at 65μm, 90μm, 140μm, and 160μm. Among these, the 90μm band, with data for 373,553 sources, emerges as the most crucial for subsequent analyses due to its heightened sensitivity.

In summary the *AKARI* PSC provides photometric information for six bands. Each datum comes with a quality indicator called Qualityflag (FQUAL). This indicator can take values from 0 to 3. FQUAL=3 is the highest quality, indicating a confirmed source. FQUAL=2 indicates a confirmed source with problems, a source with a very low flux level or a possible false detection, for example a "side-lobe" effect. FQUAL=1 implies that the source was not confirmed or that the flux value is unreliable. Finally FQUAL=0 is a non-detection. For our inquiry, we exclusively considered sources with a Qualityflag of FQUAL=3 in the 9μm, 18μm, and 90μm bands, and any Qualityflag in the 65μm, 140μm, and 160μm bands. We denote this specific combination of Qualityflag as Q33x3xx, representing the bands 9μm, 18μm, 65μm, 90μm, 140μm, and 160μm, respectively. This selection resulted in a total of 9,900 sources.

The *AKARI* photometric information was obtained from DARTS/Akari at ISAS/JAXA http://darts.jaxa.jp/ir/akari/cas/tools/ search/crossid.html using *AKARI*-CAS (Yamauchi et al. 2011).

3.2. *Catalogues for Source Discrimination*

We have cross-referenced these 9,900 sources from the *AKARI* PSC, which report high-quality photometry, against catalogues of various types of astrophysical objects from VizieR and some bibliographic references to establish correspondences. The catalogues employed for this purpose were as follows:

General catalogue of stars with the system of photoelectric astrolabes (Working Group Of GCPA 1992), Catalogued galaxies and quasars observed in the *IRAS* survey, Version 2 (Fullmer & Lonsdale 1989), New OH/IR stars from color-selected *IRAS* sources. 3: A complete survey (Chengalur et al. 1996), Pre-main sequence star Proper Motion Catalogue (Ducourant et al. 2005), Transitional YSOs (Young Stellar Objects) candidates from flat-spectrum *IRAS* sources (Magnier et al. 2000), A General Catalogue of Herbig-Haro Objects, 2nd Edition (Reipurth 2000), A catalogue of symbiotic stars (Belczynski et al. 2001), A New Catalogue of Radio Compact H II Regions in the Milky Way. II. The 1.4 GHz Data (Giveon et al. 2005), Galactic Planetary Nebulae and their central stars. I. An accurate and homogeneous set of coordinates (Kerber et al. 2004), MASH (Macquarie/AAO/Strasbourg H_α) Catalogues of Planetary Nebulae (Parker et al. 2006), Torun catalogue of post-AGB (post-Asymtotic Giant Branch) and related objects (Szczerba et al. 2007), A Mid-Infrared Imaging Survey of Proto-Planetary Nebula Candidates (Meixner et al. 1999), Possible new planetary nebulae in the *IRAS* Point Source Catalogue (Preite-Martínez 1988) and *IRAS* identification of Post-AGB and PNe candidates (Ramos-Larios et al. 2009). The selection was carried out with the aim of encompassing a broad variety of astronomical objects, facilitating a comprehensive comparison of their infrared emissions and positions in color-color maps, in relation to the emission and position of PNe and PPNe.

3.3. *Color–Color Diagram*

After reviewing the work of García-Lario et al. (1990), taking into account the available AKARI

bands, and thoroughly exploring potential color combinations, we have chosen the following color definitions.:

$$x = \log \frac{F(18\mu m)}{F(90\mu m)},$$

and

$$y = \log \frac{F(9\mu m)}{F(18\mu m)}.$$

In Figure 1, we have plotted the values for $\log[F(18\mu m)/F(90\mu m)]$ against $\log[F(9\mu m)/F(18\mu m)]$ for the 9,900 sources in the *AKARI* PSC with photometry quality Q33x3xx. Superimposed symbols represent objects also present in the catalogues mentioned above (§ 3.2). The diagram delineates distinct areas corresponding to different types of objects. Notably, there is a defined region (marked by the yellow line) where known PNe and PNe candidates are concentrated. This region, referred to as the PNe region, is situated between:

$$0.1 \leq \log \frac{F(18\mu m)}{F(90\mu m)} \leq 5,$$

and

$$0.01 \leq \log \frac{F(9\mu m)}{F(18\mu m)} \leq 0.1.$$

In addition to the objects from the catalogues of known PNe and PNe candidates, only two objects from the 'New Catalog of Radio Compact H II Regions in the Milky Way' are located in the PNe region. No objects from any of the catalogues representing other types were identified in this region. The PNe region includes 215 sources from the *AKARI* PSC with Q33x3xx. Excluding the previously identified PNe, there are 67 sources that can in principle be regarded as potential PNe candidates (Table 1).

The selection of these limits is conservative. Confirming the proposed candidates in this study could warrant an extension of the PN region, particularly by increasing the value on the ordinate axis to 0.2 to encompass more potential candidates. However, this adjustment might introduce a risk of potential contamination of the PN region with galaxies.

4. SIMBAD SOURCES

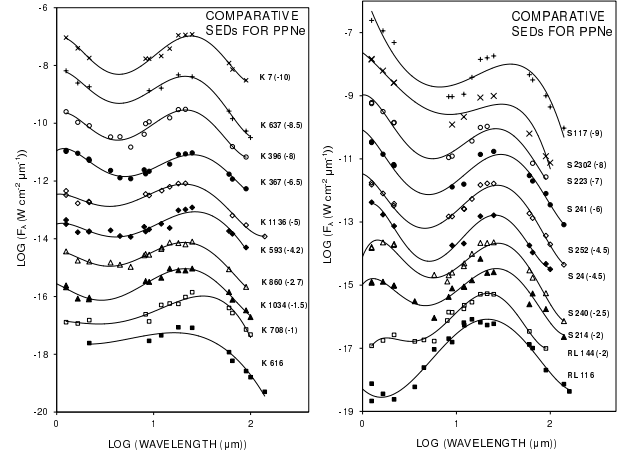We referred to the SIMBAD database to gather information about our 67 potential candidates, as

Fig. 2. SEDs of established PPNe. The double-component structure is clearly seen in the SEDs. Each PPN is identified by the initials of the authors of the corresponding catalogues: Kerber, Szczerba, and Ramos-Larios, followed by the corresponding identification number. In order to avoid overlaps between different SEDs, an offset has been applied; the value of the offset is given in brackets after the PPN name.

presented in Table 1. The search radius was set at 6 arcsec.

Out of the 67 potential candidates, 30 did not yield any identification, while in 37 cases at least one identification was obtained. Table 1 provides details such as the IRC identifier number, galactic coordinates, right ascension, declination, the SIMBAD identification, distance between the IRC source and the SIMBAD identification, and the concise SIMBAD object type (`http://simbad.u-strasbg.fr/simbad/sim-display?data=otypes`).

The total number of identifications is 50 (there may be more than one per object), of which 13 are infrared sources (IR), 7 maser sources (Mas), 7 possible PNe (PN?), 4 post-AGB candidates (pA?), 3 stars (*), 3 radio sources (Rad), 2 emission-line stars (Em*), 2 semi-regular pulsating stars (sr*) and 1 identification of each of the following types of objects: post-AGB-PPN (pA*), peculiar star (Pe*), variable star (V*), young stellar object candidate (Y*?), 'region defined in the sky' (reg), carbon star (C*), young stellar object (YSO), emission object (EmO) and high mass X-ray binary (HXB).

As a PN is an ionized circumstellar shell around a hot compact star, in the process of evolving between the AGB and white dwarf (WD) phase, it can be described in various ways depending on the particular characteristic under study. For example, it may be described as a transition object (pA* or pA?) while the central star is ionizing the envelope, the spec-

TABLE 1

AKARI PLANETARY NEBULAE CANDIDATES

No	IRC	G.C.	RA (2000) H M S	DEC (2000) D M S	IDENTIFICATION	DIST arcsec	TYPE
1	200475060	G001.30+04.07	17 33 13.13	-25 40 17.7	-	-	-
2	200557576	G006.43-01.92	18 07 31.86	-24 20 21.1	-	-	-
3	200455657	G008.55+11.49	17 23 11.65	-15 37 15.9	[M81] I-556	2.36	Em*
					IRAS 17203-1534	3.85	pA*
4	200535439	G008.85+01.69	17 59 05.08	-20 27 24.4	SCHB 258	0.61	Mas
5	200556938	G009.10-00.39	18 07 20.97	-21 16 11.2	SCHB 292	0.37	Mas
					IRAS 18043-2116	3.49	IR
6	200562588	G011.41+00.43	18 09 04.73	-18 50 42.6	*IRAS* 18061-1851	4.4	IR
7	200585006	G014.03-00.66	18 18 22.46	-17 04 00.6	-	-	-
8	200580061	G015.70+00.77	18 16 25.80	-14 55 13.0	-	-	-
9	200605366	G017.01-01.23	18 26 15.79	-14 42 26.5	OH 17.0 -1.2	2.46	Mas
					[TVH89] 301	2.46	Mas
					PN PM 1-232	5.17	PN?
10	200600445	G020.41+01.11	18 24 18.70	-10 36 30.2	*IRAS* 18215-1038	2.76	IR
11	200627833	G020.51-02.07	18 35 59.44	-11 59 39.1	-	-	-
12	200628891	G025.26+00.25	18 36 29.20	-06 42 46.7	GSC 05124-02611	1.18	*
13	200637610	G027.54+00.41	18 40 06.57	-04 36 41.9	-	-	-
14	200643853	G028.34+00.12	18 42 37.09	-04 02 04.7	-	-	-
15	200686203	G030.09-04.74	19 03 09.52	-04 41 08.4	-	-	-
16	200675903	G036.07-00.17	18 57 46.14	02 43 09.3	-	-	-
17	200700351	G036.41-03.68	19 10 54.42	01 24 41.6	2MASS J19105453+0124450	0.5	Pe*
18	200689042	G036.43-01.91	19 04 38.65	02 14 23.7	PK 036-01 3	2.4	PN?
19	200680582	G037.28-00.23	19 00 10.88	03 45 48.7	[WBH2005] G037.278-0.226	1.27	Rad
					V* V1672 Aql	1.61	V*
					2MASS J19001104+0345511	3.51	IR
20	200703532	G038.56-03.11	19 12 47.88	03 34 40.4	-	-	-
21	200704956	G042.90-01.08	19 13 37.89	08 21 47.9	-	-	-
22	200697923	G043.03+00.14	19 09 30.06	09 02 25.9	GPSR 043.028+0.140	0.75	Rad
					MSX6C G043.0281+00.1406	1.11	PN?
23	200754442	G052.24-06.42	19 51 00.78	13 58 20.4	V* TW Aql	5.44	sr*
24	200732448	G057.11+01.46	19 32 13.50	22 04 57.6	2MASS J19321348+2204566	0.99	Y*?
25	200734399	G057.81+01.46	19 33 41.50	22 42 02.8	PN PM 1-306	5.34	PN?
26	200765758	G068.20+00.24	20 01 59.87	31 03 09.9	*IRAS* 20000+3054	4.8	IR
27	200775563	G072.25+00.26	20 12 17.32	34 28 10.6	-	-	-
28	200500801	G077.13+30.87	17 44 55.03	50 02 40.2	V* V814 Her	4.25	sr*
29	200789311	G077.92+00.22	20 28 30.55	39 07 02.3	OH 2026+38	0.96	Rad
30	200796994	G080.94+00.02	20 38 49.61	41 25 22.0	-	-	-
31	200778777	G083.19+06.64	20 15 57.33	47 05 34.5	-	-	-
32	200808628	G083.61-02.20	20 57 03.78	42 06 26.6	-	-	-
33	200828078	G096.54+01.36	21 35 43.92	53 53 12.4	-	-	-
34	200862609	G111.71-02.13	23 23 13.49	58 48 05.0	[PF2007] R3	5.04	reg
35	200866080	G113.89-01.60	23 38 13.11	59 58 42.7	-	-	-
36	200865230	G115.21+04.32	23 34 21.97	66 01 56.5	*IRAS* 23321+6545	5.72	C*
37	200033305	G135.28+02.80	02 43 28.32	62 57 05.5	-	-	-
					MSX6C G200.0789-01.6323	5.19	Y*O

TABLE 1. CONTINUED

No	IRC	G.C.	RA (2000) H M S	DEC (2000) D M S	IDENTIFICATION	DIST arcsec	TYPE
38	200044584	G140.48+06.04	03 37 28.74	63 06 27.2	PN PM 1-8	2.44	PN?
					MSX6C G200.0789-01.6323	5.19	Y*O
39	200184830	G282.84-01.25	10 11 16.59	-57 44 10.6	-	-	-
40	200194383	G286.32-00.70	10 36 01.61	-59 07 44.6	*IRAS* 10341-5852	3.93	IR
					HD 303122	4.76	*
41	200193271	G286.60-01.92	10 33 05.11	-60 19 48.9	HD 305298	2.6	*
42	200200079	G289.36-02.65	10 50 20.48	-62 17 09.5	SPH 100	4.12	EmO
					IRAS 10484-6201	4.38	IR
43	200212827	G292.89-01.20	11 23 11.95	-62 20 25.8	-	-	-
44	200215868	G293.45+00.07	11 31 08.80	-61 19 07.0	-	-	-
45	200212510	G294.04-04.71	11 22 18.58	-66 01 46.8	*IRAS* 11201-6545	4.35	pA?
46	200235503	G299.54-00.02	12 21 45.12	-62 41 50.1	*IRAS* 12190-6225	2.71	IR
47	200246253	G302.55-02.74	12 47 46.78	-65 36 41.3	PN PM 1-69	2.43	PN?
48	200254043	G304.57+00.72	13 05 27.82	-62 06 37.4	-	-	-
49	200259071	G305.79+00.28	13 16 11.59	-62 27 14.2	*IRAS* 13129-6211	1.88	IR
50	200279625	G311.02+02.03	13 56 24.00	-59 48 59.3	*IRAS* 13529-5934	4.96	pA?
51	200285648	G311.68-00.63	14 07 35.16	-62 11 47.3	-	-	-
52	200302084	G313.87-04.08	14 36 34.50	-64 41 31.5	*IRAS* 14325-6428	0.89	pA?
53	200314558	G316.94-02.88	14 56 46.81	-62 17 29.9	-	-	-
54	200323862	G320.68+00.25	15 10 43.74	-57 44 47.7	*IRAS* 15068-5733	3.6	IR
55	200327862	G321.02-00.70	15 16 41.23	-58 22 28.6	*IRAS* 15127-5811	3.2	IR
56	200354340	G325.16-03.01	15 52 19.68	-57 50 52.5	*IRAS* 15482-5741	4.31	pA?
57	200366578	G331.16+00.78	16 06 40.62	-51 03 56.4	OH 331.16 +0.78	1.35	Mas
58	200365730	G332.29+02.28	16 05 41.23	-49 11 33.8	Caswell OH 332.295+02.280	5.79	Mas
					Caswell CH3OH 332.295+02.280	5.98	Mas
59	200392246	G335.06-01.16	16 32 39.87	-49 42 14.0	EM* VRMF 55	0.78	Em*
					IGR J16327-4940	0.78	HXB
					IRAS 16288-4935	4.69	IR
60	200397316	G335.95-01.36	16 37 14.40	-49 11 19.0	PN G335.9-01.3	3.67	PN?
61	200389424	G336.24+00.51	16 30 10.70	-47 42 37.8	-	-	-
62	200412657	G340.43-00.37	16 50 08.91	-45 09 26.4	-	-	-
63	200420643	G342.44-00.23	16 56 39.52	-43 30 49.6	-	-	-
64	200413826	G350.43+07.61	16 51 06.42	-32 23 00.5	-	-	-
65	200422895	G352.57+07.30	16 58 27.11	-30 55 06.3	2MASS J16582725-3055108	4.98	IR
66	200489617	G355.61-01.16	17 39 27.29	-33 16 41.2	-	-	-
67	200571327	G359.81-06.87	18 12 58.61	-32 30 04.1	-	-	-

trum of which shows strong emission lines (Em*) including those of ionized hydrogen (H II), the material expelled during the AGB mass-loss phase is heated by radiation or shocks, and therefore is an IR source (IR), and this material can contain large quantities of carbon, product of the triple-α reaction (C*). Besides, the central stars of PNe, which are terminating their AGB phase, can have brightness variations (sr* and V*). Also, the PPNe can show maser emission (Mas) due to the presence of water (Uscanga et al. 2019), and finally some rotational molecular transitions emit at radio wavelengths (Rad). So all these classifications do not rule out the possibility of the objects being PN or PPN candidates. Therefore, objects thus identified are not excluded from the potential candidate list.

On the other hand, classifications such as star (*), peculiar star (Pe*), region defined in the sky (reg) and emission object (EmO) are poorly defined and are not sufficient reasons to exclude sources with such classifications from the potential candidate list.
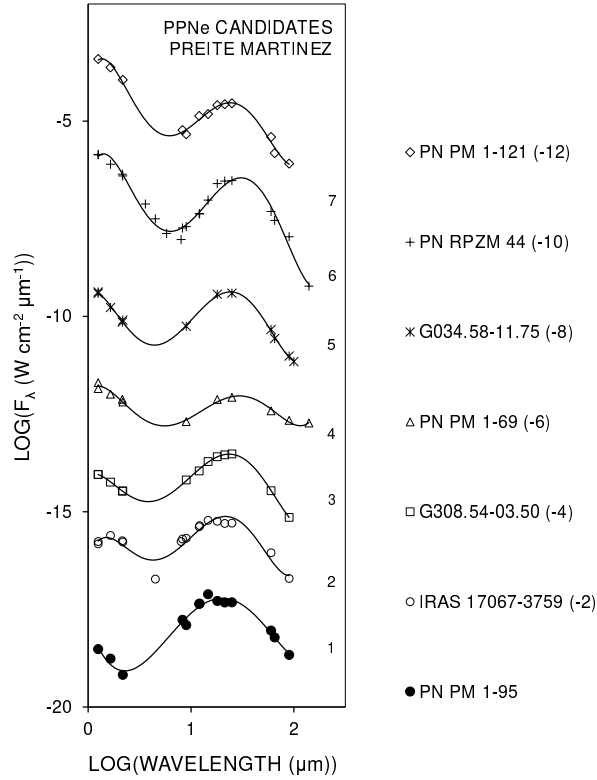
Fig. 3. SEDs of PPN candidates from Preite-Martínez (1988). The double-component structure is also clear in these candidates. In order to avoid overlaps between different spectra, an offset has been applied to the spectra. The value of the offset is given in brackets after the PPN name.

5. SPECTRAL ENERGY DISTRIBUTIONS

It is anticipated that the 67 candidates identified as PN will exhibit a range of evolutionary states. We intend to explore these states through a comprehensive analysis of their SEDs. PNe in their formative stage, known as PPNe, possess an envelope that is still in the process of expansion. In the initial stages, the envelope exhibits a nearly uniform temperature, leading to emissions with a profile closely resembling that of a black body corresponding to a specific temperature. Furthermore, the central star of the planetary nebula (CSPN) emits with a black body profile corresponding to a distinct temperature. In this initial phase, the outcome is what Kwok (2000) refers to as a two-component SED. Here, the cooler component aligns with the envelope expelled during the asymptotic giant branch (AGB) phase, while the warmer component corresponds to the stellar photosphere. Following this, as the envelope expands, its temperature gradient will intensify. The overall emission will then be a cumulative effect of multiple layers, each at a distinct temperature, along with the emission from the star. The peak emission from the star will shift towards longer wavelengths (Hrivnak, Kwok, & Volk (1988), Hrivnak, Kwok, & Volk (1989)).

To characterize the potential candidates, we utilized photometry across various observational projects, encompassing wavelengths from the blue, at $0.44\mu m$ (USNO B1 + B2), to the far-infrared (FIR) at $160\mu m$ (*AKARI* FIS) (see Section 2: Observations, for details). It is crucial to highlight that the photometric data from the USNO frequently produced outcomes that displayed disparities with those acquired from other telescopes. Consequently, this specific dataset was omitted from the construction of the SEDs for the associated sources.

Furthermore, we produced comparable SEDs for well-established PNe and PPNe, serving as a control cohort. Figure 2 illustrates the SEDs of confirmed PPNe, displaying their distinctive two-component architecture. Likewise, Figure 3 showcases the SEDs of seven PPNe candidates identified by Preite-Martínez (1988).

Figures 4, 5, and 6 illustrate the SEDs of 49 candidates displaying a two-component structure. We shall refer to this ensemble of 49 candidates, whose SEDs align with those of known PPNe, as Group A. For presentation purposes, we have subdivided Group A into five sets, labelled A1 to A5. In A1 and A2 (Figure 4), the SEDs are primarily influenced by the emission peak at shorter wavelengths, signifying the hotter component, i.e., the central star. In A3

There are only three additional classifications corresponding to G057.11 +01.46, G140.48 +06.04 and G335.06 –01.16 (numbers 24, 38, and 59, respectively, in Table 1). The first source is designated as a candidate young stellar object (Y*?), but due to its unconfirmed status, we do not exclude it. The second source carries an additional classification as a PN candidate (PN?), which is why it remains in the list. The third is identified as a high-mass X-ray binary (HXB) and is also classified as an emission-line star (Em*) and an IR source (IR), the last two being consistent with PN candidacy.

Utilizing information from SIMBAD, there is no justification to exclude any of the 67 sources from the list of potential PNe candidates. Following this we present a thorough analysis of their spectral energy distributions (SEDs) to discern their possible evolutionary state, complemented by a morphological examination of the sources and an assessment of their environment using archival images.
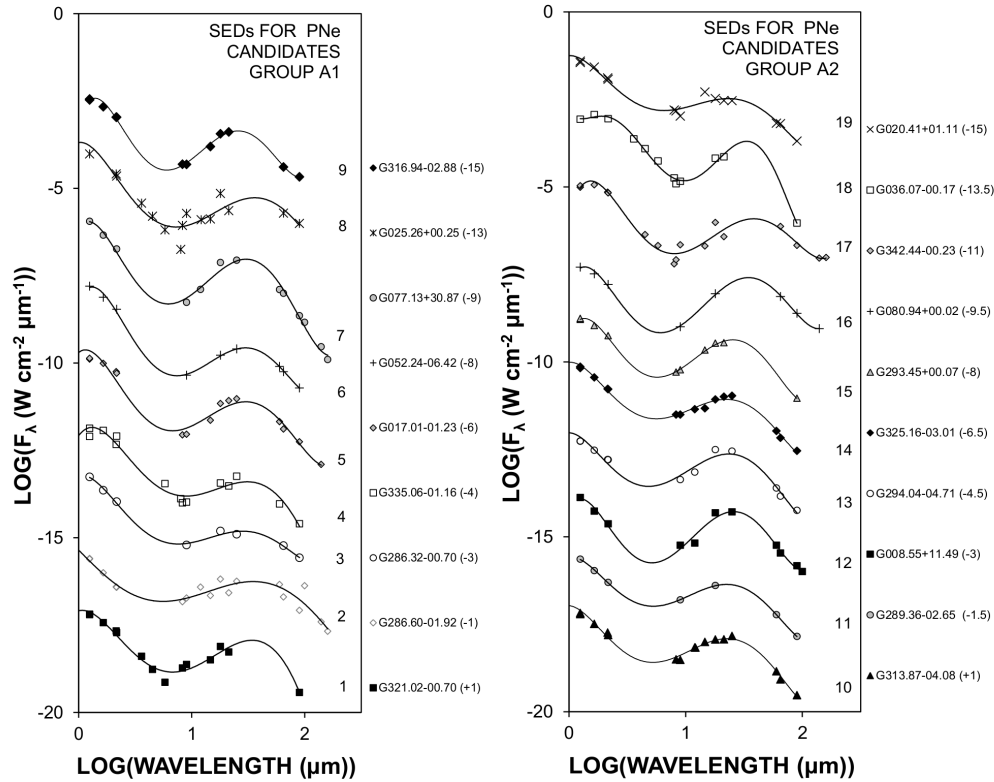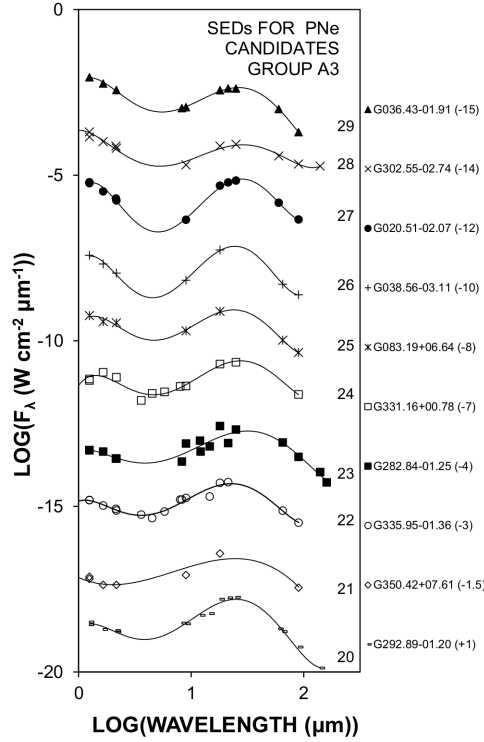
Fig. 4. SEDs of 19 candidates in PNe group A, which show the double-component structure characteristic of PPNe with a dominance of the hot component.

(Figure 5), the SEDs display a relatively balanced emission from both components, while A4 and A5 (Figure 6) predominantly exhibit emissions from the cooler component, i.e., the envelope.

On the contrary, a distinct subset of candidates presents a discernible SED pattern, reminiscent of more advanced PNe that do not exhibit distinct components. Instead, they exhibit collective emissions from multiple layers, each distinguished by its individual black-body radiation. Figure 7 illustrates the SEDs of three objects previously identified by Preite-Martínez (1988) as PNe showcasing this SED profile. In Figure 8, we depict the SEDs of potential PN candidates characterised by an SED featuring only one peak. This subset of candidates, referred to as Group B, represents the more evolved candidates for PNe.

6. MORPHOLOGY AND PROFILES

In our initial endeavor to verify the nature of potential candidates, we examined the images from the *AKARI* far-infrared all-sky survey maps. However, the pixel scale of the detectors, measuring $26.8'' \times 26.8''$ for the short wavelength bands N60 and WIDE-S, and $44.2'' \times 44.2''$ for the long wavelength bands N160 and WIDE-L (Doi, et al. 2015), proved insufficient for drawing definitive conclusions. Consequently, we turned to the observations from *WISE* (Wide-Field Infrared Survey Explorer, Wright et al. 2010), to conduct an initial morphological study. This approach aids us in reviewing the list of potential candidates.

Figures 9, 10 and 11 present RGB images of the 67 potential candidates combining the W1 (in blue), W2 (green) and W3 (red) bands. Upon close examination of the RGB images, a noteworthy observation is that the majority of objects exhibit significant obscuration in the W1 and W2 bands, in comparison to the W3 band. This characteristic is not observed in only two sources: G083.19+06.64 and G140.48+06.04 (Figure 10, Row 2, Column 3 and Row 4, Column 2 respectively). For the remaining sources, the prevalence of the W3 band is evident, ranging from subtle, in the case of G077.13+30.87, to remarkably pronounced, as observed in G352.57+07.30. Another common feature among the majority of these sources is their

Fig. 5. SEDs of 10 candidates in PNe group A, which show the double-component structure characteristic of PPNe with a relative balance between the cold and hot components.

radial symmetry, with the sole exception being G342.44-00.23. Two sources warrant additional commentary, G111.71-02.13 and G113.89-01.60 (Figure 10, Row 3, Columns 2 and 3 respectively). G111.71-02.13 appears to be associated with a larger arc-like structure and does not exhibit a star-like appearance. In Figure 12 a broader section of the sky encompassing this source is depicted (FoV 3.2'), with the highlighted area inside the white square corresponding to the segment presented in Figure 10. It is evident that G111.71-02.17 effectively constitutes a component of a supernova remnant (SNR), precisely identified as the SNR G111.7-02.1, commonly referred to as Cassiopeia A (Cas A). This enables us to exclude this source from the ultimate candidate list. On the other hand G113.89-01.60 seems to represent an emission peak within an arc encircling the star LS I +59 10, documented in the literature as a B0.2III spectral type star (Negueruela & Marco 2003). It is plausible to categorize G113.89-01.60 as a component of the HII region LBN 113.05-04.51, associated with LS I +59 10, and thereby, we can remove it from our candidate list too.

Furthermore, we have examined potential instances using *Spitzer* IR images acquired with IRAC. In cases where IRAC images were unavailable, we turned to 2MASS images, aiming to identify morphologies consistent with extended emission of PNe, such as lobe structures, equatorial disks, or other PN-like configurations. Due to the limited resolution of 2MASS, we have opted to choose only certain cases of particular interest. Figure 13 shows RGB images of nine sources, five from *Spitzer* and four from 2MASS. For each instance, the orientation is set with North at the top and East to the left. The lower left corner of each image provides information about the data source, the lower right corner indicates the object name, and a scale bar is incorporated for reference.

In Figure 13, five sources-G083.61-02.20, G113.89-01.60, G332.29+02.28, G027.54+00.41, and G135.28+02.80-exhibit a notably dense envelope that prevails over the central emission. Regarding this, the first two are the most prominent, where the radiation from a possible central star is totally absorbed by a spherical-type envelope; but G113.89 –01.60 appears in Figure 10, Row 3, Column 3 to be an extended part of another source, while G083.61 –02.20 presents an E-W structure. In the other three cases mentioned above, we observe a clear bipolar structure with progressively more emission in the centre, but this central emission does not dominate the lobe emission. These five sources are part of our group B of the general candidate list.

On the other hand, the images of G304.57 +00.72, G311.68 –0.63, G025.26 +00.25 and G321.02 –00.70 show dominant central stars. In the first two cases we see spherical envelopes absorbing the emission of the central star. In both images we observe the envelope heated by the stellar radiation, although, as we can see in their respective SEDs (Figure 6, group A4, 38 and 37), the stellar emission is still important and its emission peak can be distinguished. Meanwhile, the image of G025.26 +00.25, although presenting an envelope similar to G304.57 +00.72 and G311.68 –00.63, has subtle differences which have important effects in its emission. The star is not situated in the center of the envelope, which allows part of the stellar emission to escape. In the corresponding SED (Figure 4, group A1, number 8) the dominant component is the high-temperature one (central star). Finally, the image of G321.02 –00.70 shows a structure clearly reminiscent of bipolar PNe. The emission from the central star dominates the combined emission from both lateral structures located to the NE and SW,
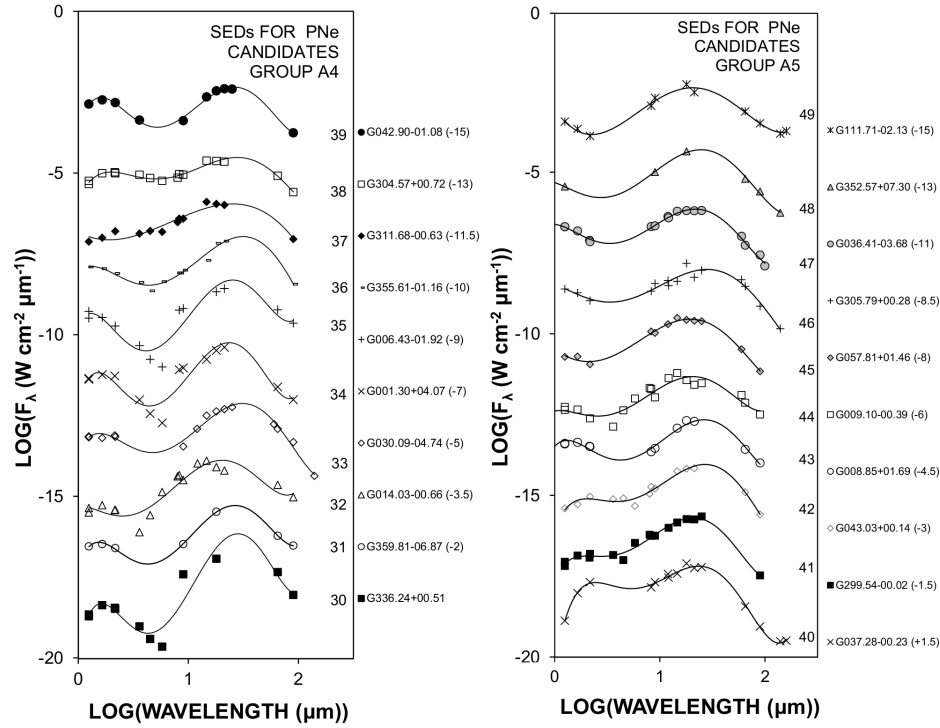
Fig. 6. SEDs of 20 candidates in PNe group A, which show the double-component structure characteristic of PPNe with a dominance of the cold component.
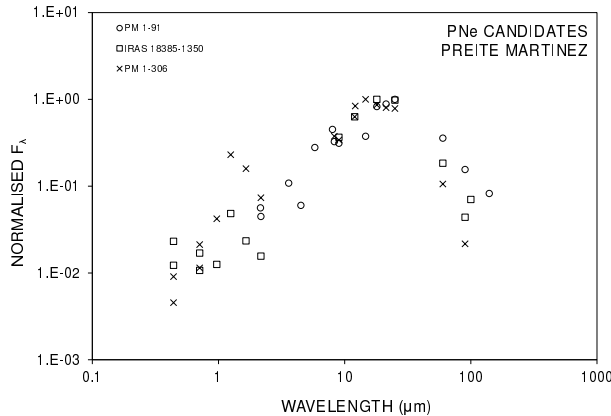

Fig. 7. SEDS of PN from Preite-Martínez (1988). More evolved PNe which do not have a SED of two components, but have layers with a continuous distribution of temperatures.

Fig. 8. SEDs of candidates in PNe group B, which have a more advanced evolutionary state.

as can be seen in its SED (Figure 4, A1, 1), which shows that the hot component clearly dominates the cold one.

We have conducted a comprehensive examination of the spatial distribution of the emission across multiple available bands for a subset of the candidates. The extracted profiles are depicted in Figure 14.

The profiles of G113.89 −01.60 and G083.61 −02.20 show that these are extended sources. In particular the profile of G113.89 −01.60 has K-band emission with a width of ≈ 22 arcsec, but this emission appears in Figure 10, Row 3, Column 3 as an extended part of another source. G083.61 −02.20 has a width of ≈ 10 arcsec in the three 2MASS bands. G027.54 +00.41 and G332.29 +02.28 show an elongated emission profile, which is expected for PNe
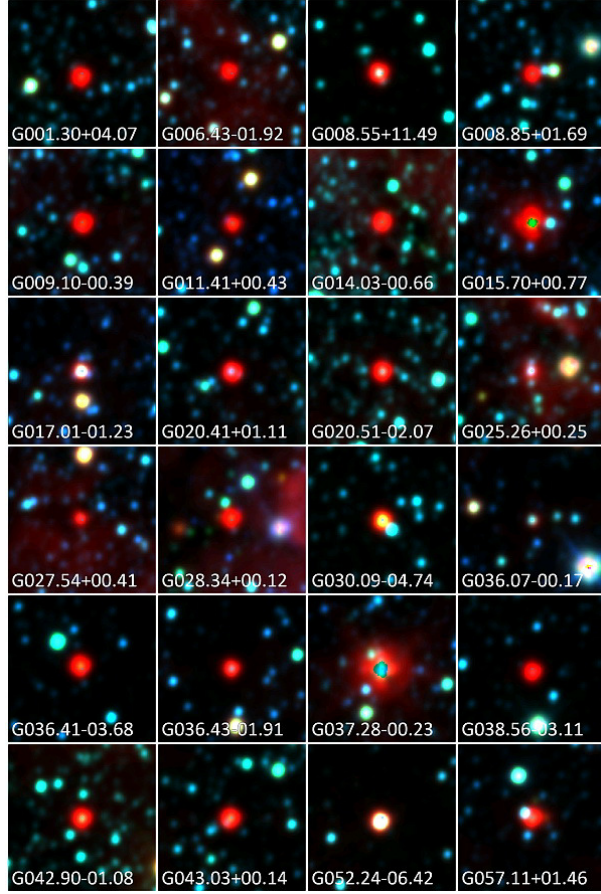
Fig. 9. RGB images of PNe candidates 1 to 24. RGBs constructed with *WISE* bands 3.4µm (blue), 4.6µm (green) and 12µm (red). In all images north is up, east to the left, and FoV 3.2'. The color figure can be viewed online.
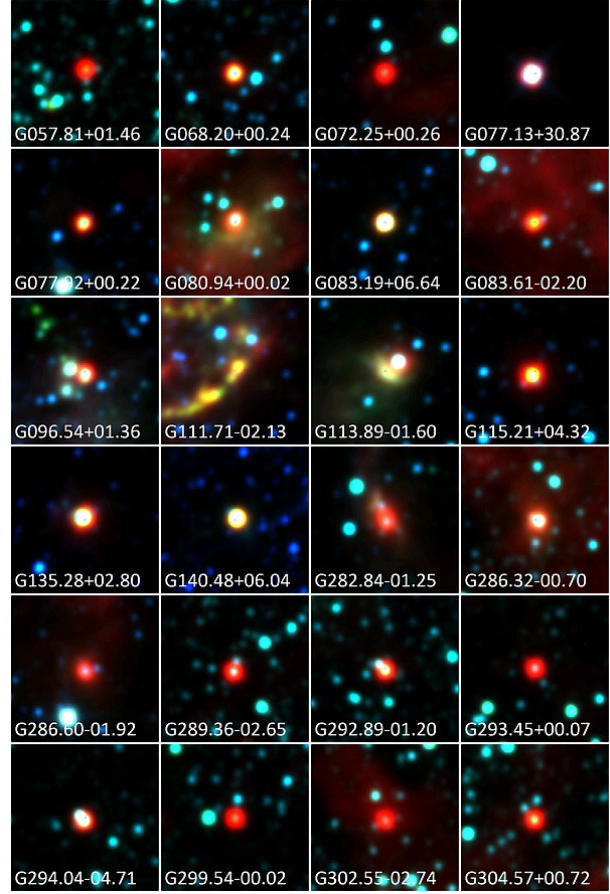

Fig. 10. RGB images of PNe candidates 25 to 48. RGBs constructed with *WISE* bands 3.4µm (blue), 4.6µm (green) and 12µm (red). In all images north is up, east to the left, and FoV 3.2'. The color figure can be viewed online.

with a certain degree of evolution, and this seems to be supported by the SEDs of both objects in Figure 8. In both cases the images also show the elongated structure characteristic of bipolar PNe.

G135.28 +02.80 and G025.26 +00.25 also show extended profiles, although with convex-shaped sides which appear to be layers expelled from the central region. In G135.28 +02.80 the convex-shaped sides are quite symmetric, which suggests that the central area is embedded in a dusty envelope, while in the case of G025.26 +00.25 this envelope is clearly asymmetric, permitting the emission of the possible CSPN to escape freely, which is confirmed by its SED (Figure 4, A1, 8). Finally the profiles of G311.68 –00.63 and G304.57 +00.72 show slightly extended emission in the four IRAC bands, especially at 5.8µm and 8.0µm. This can be explained by a layer of expelled dust, which can be confirmed using their

SEDs (Figure 6, A4, 37 and 38 respectively), where two similar-strength components of thermal emission can be seen.

7. INDEPENDENT CONFIRMATION OF G050.48 –00-70

One of the sources within the PN region (Figure 1) that has been excluded from the current list of candidates is G050.48 -00.70. This object was previously identified as a PN by Urquhart et al. (2009), in a study on YSOs that is entirely independent of the analysis conducted here. To verify this classification, we present images (Figure 15) and emission profiles (Figure 16) of G050.48 –00.70 from *Spitzer*/IRAC, 2MASS and IPHAS. The Hα emission reveals significant extinction in its central region (Figure 15, above), with a pair of symmetric 'cones' of emission escaping from the high extinction region. This sug-
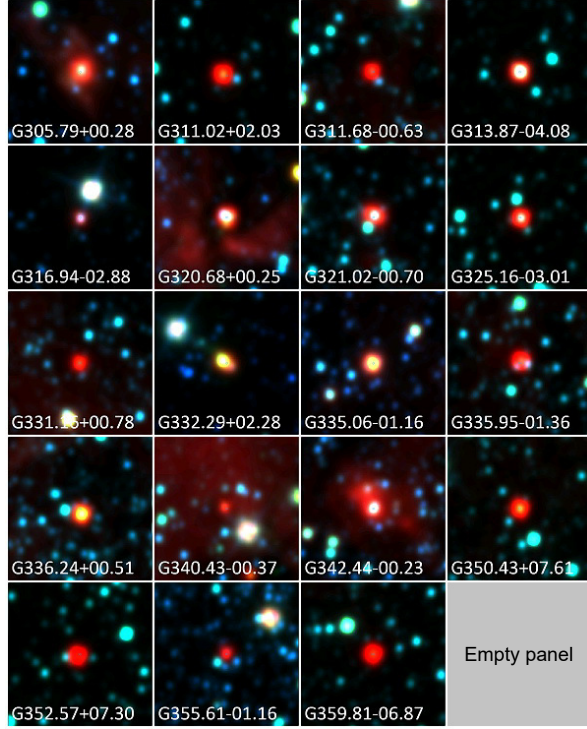
Fig. 11. RGB images of PNe candidates 49 to 67. RGBs constructed with *WISE* bands 3.4µm (blue), 4.6µm (green) and 12µm (red). In all images north is up, east to the left, and FoV 3.2'. The color figure can be viewed online.

gests the presence of dusty material in the center and ionized material in the cones. The color-composite image with J (blue), H (green) and K (red) from 2MASS (Figure 15, center) exhibits strong emission in the center of the cones and between them at shorter wavelengths, while K-band emission dominates at the edges. This indicates that the conical structures are being heated from the central region. Finally the color-composite image with bands 4.5µm (blue), 5.8µm (green) and 8.0µm (red) from *Spitzer*/IRAC (Figure 15, below) illustrates emission concentrated in the central region across all three bands.

In particular, the emission at 8.0µm indicates heated dust, which is the same material that causes the extinction in Hα, then re-emitting at 8.0µm. All the above can be seen in the graphical representation of the emission profiles in Figure 16, which contains the Hα profiles, the 3 bands of 2MASS and the four from *Spitzer*/IRAC. Therefore, from the PSC photometry of *AKARI*, and the morphology and emission profiles in the optical, NIR and FIR, we can conclude independently of Urquhart et al. (2009) that G050.48 +00.70 is a PN.
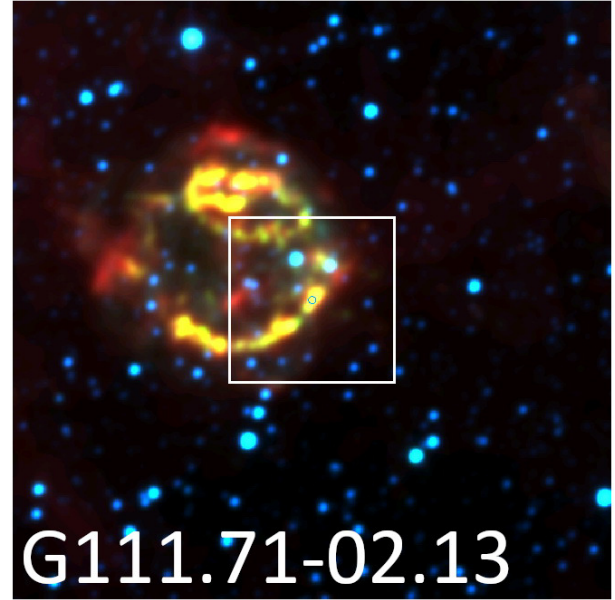
Fig. 12. Wide RGB images of PNe candidate G111.71-02.13. RGBs constructed with *WISE* bands 3.4µm (blue), 4.6µm (green) and 12µm (red). North is up, east to the left, and the total FoV is 12' while the white box encloses the frame shown in Figure 10 with FoV of 3.2'. The color figure can be viewed online.
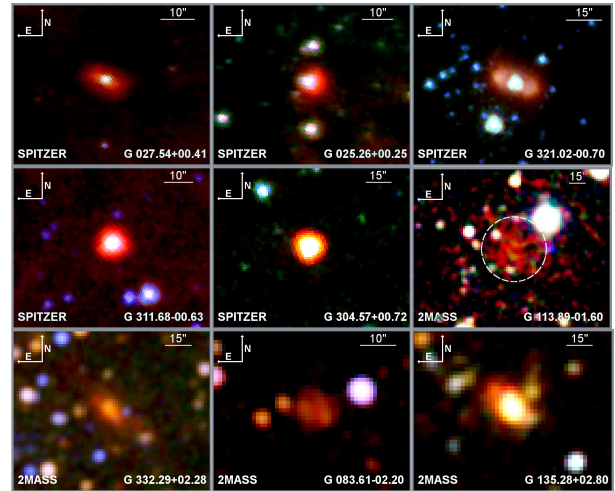

Fig. 13. RGB image of PNe candidates. The RGBs constructed from *Spitzer* images use the 4.5µm (blue), 5.8µm (green) and 8.0µm (red) bands, while those from 2MASS use the 1.25µm (blue), 1.65µm (green), and 2.17µm (red) bands. The color figure can be viewed online.

8. CONCLUSIONS

By analyzing the *AKARI* photometry and other instruments employed in this study, we can draw the following conclusions.
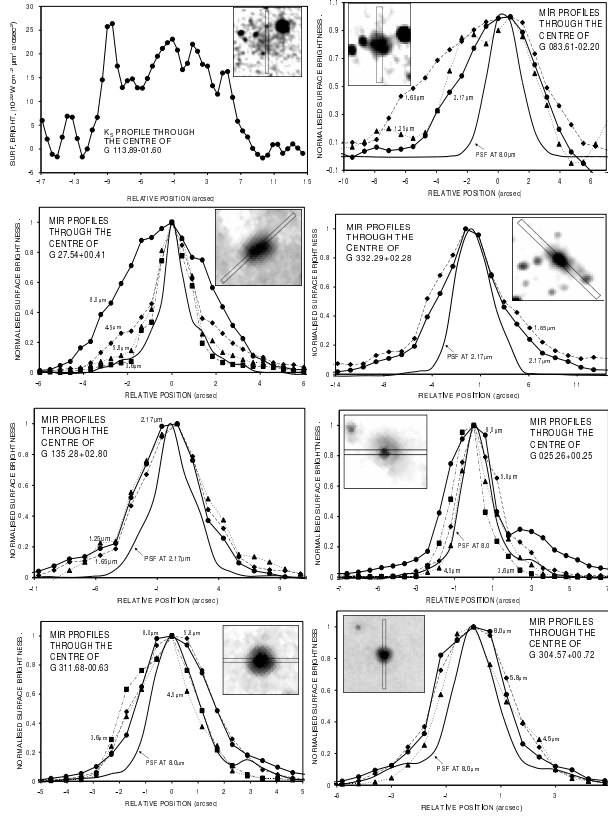
Fig. 14. Spatial profiles of selected candidates. We have extracted spatial profiles along an axis through the center of a sample of candidates, in order to study the spatial distribution of the emission and determine whether they are extended sources.

(i) The photometry in the $9\mu m$, $18\mu m$ y $90\mu m$ AKARI bands enables the determination of color indices that are effective in discriminating between PNe-type sources, and other astronomical objects.

(ii) At least 67 sources from the AKARI PSC exhibit emission characteristics consistent with PNe or related objects, yet they haven't been definitively identified as such in the existing literature. We consider these as potential candidate PNe and/or PPNe.

(iii) Examination of the SEDs of the potential candidates facilitates their categorization into two groups based on their evolutionary stage, PPNe and PNe.

(iv) Visual inspection of images allows us to exclude two sources, G113.89-01.60, identified as part of a stellar envelope, and G111.71-02.13, associated with the Cassiopeia A SNR.

(v) Finally, after the elimination of two potential candidates, we propose 65 sources from the AKARI PSC as PNe or PPNe candidate.
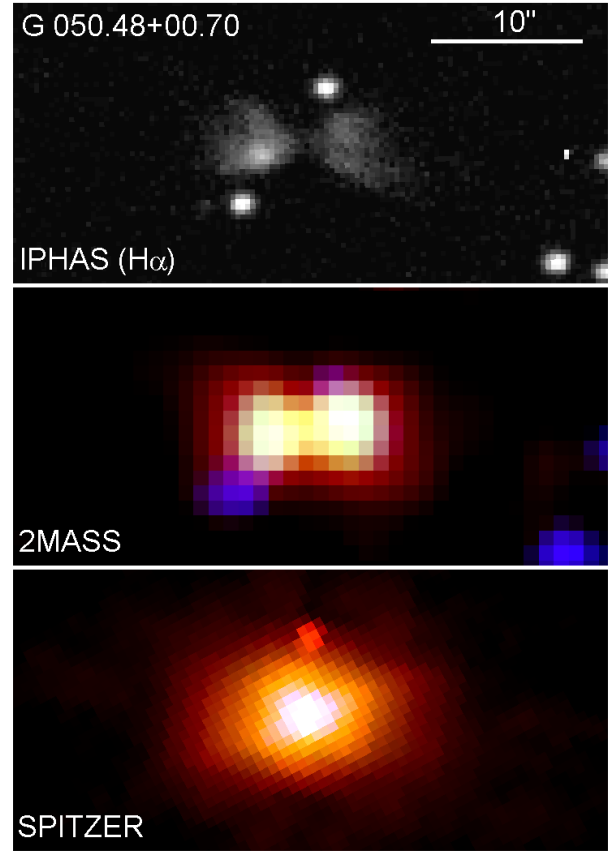

Fig. 15. Images of G050.48 +00.70. Above: Hα λ656.3nm from IPHAS. Center: Composite color image with J (blue), H (green), K (red) from 2MASS. Below: Composite color image using the $4.5\mu m$ (blue), $5.8\mu m$ (green) and $8.0\mu m$ (red) bands from Spitzer/IRAC. The color figure can be viewed online.
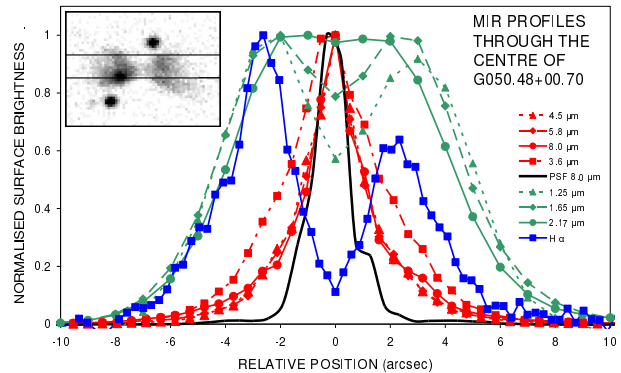

Fig. 16. Spatial profiles of G050.48 +00.70. The Hα emission profile is shown in blue, the three 2MASS bands in green and the four Spitzer/IRAC bands in red. Each 2MASS and Spitzer/IRAC band is identified by different geometric shapes. The color figure can be viewed online.

Additionally, we propose two avenues for future research. Firstly, a spectroscopic examination of the 65 final candidates to either validate or discard their candidacy. Secondly, a reconsideration of the limits used to define the planetary nebulae (PNe) region in our color-color diagram. If the majority of the 65 candidates presented here are substantiated, it would be valuable to expand the boundaries of the PN region, encompass more sources, categorize them, and subject them to thorough analysis of images and spectra for confirmation or rejection as candidates.

REFERENCES

Akras S., Guzman-Ramirez L., & Gonçalves D. R., 2019, MNRAS, 488, 3238, https://doi.org/10.1093/mnras/stz1911

Akras S., Leal-Ferreira M. L., Guzman-Ramirez L., & Ramos-Larios G., 2019, MNRAS, 483, 5077, https://doi.org/10.1093/mnras/sty3359

Belczynski K., Mikolajewska J., Munari U., Ivison R. J., & Friedjung M., 2001, yCat, 4146, 60407

Chengalur J. N., Lewis B. M., Eder J., & Terzian Y., 1996, yCat, 2089, 90189, https://doi.org/10.26093/cds/vizier.20890189

Cox N., Manchado A., García-Lario P., & Szczerba R., 2009, ASPC, 418, 439, https://doi.org/10.48550/arXiv.0905.2903

Cox N., García-Lario P., García-Hernández D. A., & Manchado A., 2009, ASPC, 418, 137, https://doi.org/10.48550/arXiv.0905.2898

Cox N. L. J., García-Hernández D. A., García-Lario P., & Manchado A., 2011, AJ, 141, 111, https://doi.org/10.1088/0004-6256/141/4/111

Doi Y., Takita, S., Ootsubo, T., et al. 2015, PASJ, 67, 50, https://doi.org/10.1093/pasj/psv022

Drew J. E., Greimel, R., Irwin, M. J., et al. 2005, MNRAS, 362, 753, https://doi.org/10.1111/j.1365-2966.2005.09330.x

Ducourant C., Teixeira R., Perie J. P., Lecampion J. F., Guibert J., & Sartori M. J. 2005, yCat, 343880769, https://doi.org/10.26093/cds.vizier.34380769

Egan M. P. & Price S. D. 1996, AJ, 112, 2862, https://doi.org/10.1086/118227

Fazio G. G., Hora, J. L., Allen, L. E., et al. 2004, ApJS, 154, 10, https://doi.org/10.1086/422843

Fouqué P., Chevallier, L., Cohen, M. et al. 2000, A&AS, 141, 313, https://doi.org/10.1051/aas:2000123

Fullmer L. & Lonsdale C. J. 1989, IRASG, 0

García-Lario P., Manchado A., Suso S. R., Pottasch S. R., & Olling R. 1990, A&AS, 82, 497

Giveon U., Becker R. H., Helfand D. J., & White R. L. 2005, AJ, 129, 348, https://doi.org/10.1086/426360

Hrivnak B. J., Kwok S., & Volk K. M. 1988, ApJ, 331, 832, https://doi.org/10.1086/166603

Hrivnak B. J., Kwok S., & Volk K. M. 1989, ApJ, 346, 265, https://doi.org/10.1086/168007

Ishihara D., Onaka, T., Kataza, H., et al. 2010, A&A, 514, 1, https://doi.org/10.1051/0004-6361/200913811

Ishihara D., Onaka, T., Kataza, H., et al. 2010, yCat, 2297, 0

Kawada, M., Baba, H., Barthel, P. D., et al. 2007, PASJ, 59, 389, https://doi.org/10.1093/pasj/59.sp2.S389

Kerber F., Mignani R. P., Guglielmetti F., & Wicenec A. 2004, yCat, 340881029, https://doi.org/10.26093/cds/vizier.34081029

Kleinmann S. G. 1992, ASPC, 34, 203

Kwok S., 2000, The Origin and Evolution of Planetary Nebulae (Cambridge, UK: CUP)

Magnier E. A., Volp A. W., Laan K., van den Ancker M. E., & Waters L. B. F. M., 2000, yCat, 335220228, https://doi.org/10.26093/cds/vizier.33520228

Manchado, A., Pottasch S. R., Garcia-Lario P., Esteban C., & Mampaso A. 1989, A&A, 214, 139

Meixner, M., Ueta, T., Dayal, A. et al. 1999, ApJS, 122, 221, https://doi.org/10.1086/313215

Monet D. G., Levine, S. E., Canzian, B., et al. 2003, AJ, 125, 984, https://doi.org/10.1086/345888

Murakami, H., Baba, H., Barthel, P., et al. 2007, PASJ, 59, 369, https://doi.org/10.1093/pasj/59.sp2.S369

Negueruela, I. & Marco, A., 2003, A&A, 406, 119, https://doi.org/10.1051/0004-6361:20030605

Ohsawa, R., Onaka, T., Sakon, I. et al. 2012, PKAS, 27, 259, https://doi.org/10.5303/PKAS.2012.27.4.259

Ohsawa R., Onaka T., Sakon I., Matsuura M., & Kaneda H. 2016, AJ, 151, 93, https://doi.org/10.3847/0004-6256/151/4/93

Parker, Q. A., Acker, A., Free, D. J. et al. 2006, yCat, 5127, 0

Phillips, J. P. & Márquez-Lugo R. A. 2011, RMxAA, 47, 83

Pollo, A., Takeuchi, T. T., & Rybka P., 2011, EP&S, 63, 1051, https://doi.org/10.5047/eps.2011.04.005

Pottasch, S. R. 1984, ASSL, 107, https://doi.org/10.1007/978-94-009-7233-9

Pottasch, S. R., Bignell, C., Olling, R., & Zijlstra, A. A., 1988, A&A, 205, 248

Preite-Martínez, A. 1988, A&AS, 76, 317

Ramos-Larios, G., Guerrero, M. A., Suárez, O., Miranda, L. F., & Gómez, J. F., 2009, A&A, 501, 1207, https://doi.org/10.1051/0004-6361/200811552

Reipurth, B. 2000, yCat, 5104, 0

Szczerba, R., Siodmiak, N., Stasinska, G., & Borkowski J., 2007, yCat, 34690799, https://doi.org/10.26093/cds/vizier.34690799

Ueta, T., Szczerba, R., Fullard, A. G., & Takita, S., 2019, IAUS, 343, 522, https://doi.org/10.1017/S1743921318006452

Urquhart, J. S., Hoare, M. G., Lumsden, S. L., et al. 2009, A&A, 507, 795, https://doi.org/10.1051/0004-6361/200912608

Uscanga, L., Gómez, J. F., Yung, B. H. K., et al. 2019, IAUS 343, Why Galaxies Care About AGB Stars: A Continuing Challenge through Cosmic Time, 343, 527, https://doi.org/10.1017/S1743921318007354

Van de Steene, G. C. & Pottasch, S. R. 1993, IAUS Planetary nebulae: proceedings of the 155 Symposium of the International Astronomical Union, 155, 40

_____. 1995, A&A, 299, 238

Working Group Of GCPA, 1992, BICDS, 41, 7

Wright, E. L., Eisenhardt, P. R. M., Mainzer, A. K., et. al. 2010, AJ, 140, 1868, https://doi.org/10.1088/0004-6256/140/6/1868

Yamamura, I., Makiuti, S., Ikeda, N., 2010, yCat, 2298, 0

Yamauchi, C., Fujishima, S., Ikeda, N. et al. 2011, PASP, 123, 852, https://doi.org/10.1086/660926

Zhang, C. Y. & Kwok, S., 1991, A&A, 250, 179

L. J. Corral, S. N. Kemp, R. A. Márquez-Lugo, S. G. Navarro, A. Nigoche-Netro, and G. Ramos-Larios: Departamento de Física, Universidad de Guadalajara, Jalisco, México.

L. J. Corral, S. N. Kemp, R. A. Márquez-Lugo, S. G. Navarro, A. Nigoche-Netro, and G. Ramos-Larios: Instituto de Astronomía y Meteorología, Av. Vallarta 2602, C. P. 44130, Guadalajara, Jalisco, México (alejandro.marquez@academicos.udg.mx).